e-ISSN: 2689-4934

Available online at
http://uppp.uitm.edu.my/online-issues.html

ESTEEM Academic Journal Vol 21, March 2025, 41–58

ESTEEM Academic Journal (EAJ)

The role of xerogel in immobilising carbon quantum dots derived from oil palm mesocarp fibre: A potential adsorbent for CO_2 capture

Aimi Solihah Zaul Kapri[1], Norhusna Mohamad Nor[1*]

[1]*Centre for Chemical Engineering Studied, Universiti Teknologi MARA Cawangan Pulau Pinang, 13500 Permatang Pauh, Pulau Pinang Malaysia*

ARTICLE INFO

Article history:
Received 27 January 2025
Revised 24 February 2025
Accepted 9 March 2025
Online first
Published 24 March 2025

Keywords:
Adsorption
Carbon quantum dots (CQDs)
CO_2 removal
Mesocarp fibre
Oil palm waste
Xerogel

DOI:
10.24191/esteem.v21iMarch.4713.g3055

ABSTRACT

Carbon quantum dots (CQDs) often suffer from agglomeration and structural instability, significantly reducing their adsorption efficiency and reusability. This study investigates the role of xerogel in stabilising and immobilising CQDs derived from oil palm mesocarp fibre (MF) as a potential CO_2 adsorbent. The extracted MF cellulose was synthesised into CQDs via hydrothermal treatment and subsequently immobilised within a xerogel matrix (X-MF-CQDs). The CO_2 adsorption performance was evaluated through breakthrough and sorption capacity experiments, where X-MF-CQDs at a 1:50 dilution exhibited the highest sorption capacity (129.04 mg/g) and a moderate breakthrough time (61.3 s). BET analysis confirmed a low surface area (0.7011 m^2/g), while pore size distribution revealed dominant micro porosity (~20 Å), crucial for CO_2 capture. FTIR analysis indicated the presence of N–H, C=N, C-O, and C-S bonds, confirming successful heteroatom doping. CHNS analysis revealed a composition of 50.33 % C, 22.78 % O, and 0.6 % S, highlighting the contribution of heteroatoms in CO_2 affinity. HRTEM and FESEM analyses confirmed uniform CQDs dispersion within the xerogel matrix, effectively minimising agglomeration and enhancing adsorption. These findings demonstrate the effectiveness of xerogel-immobilised CQDs (X-MF-CQDs) as a stable and efficient CO_2 adsorbent, promoting sustainable waste valorisation strategies.

1. INTRODUCTION

Carbon dots (CDs) are generally defined as diminutive carbon nanoparticles, with size below 10 nm that remain dispersed in an aqueous solution [1]. In 2004, carbon dots (CDs) were first discovered as a by

[1*] Corresponding author. *E-mail address*: norhusna8711@uitm.edu.my
https://doi.org/10.24191/esteem.v21iMarch.4713.g3055

product of purifying single-walled carbon nanotubes. By 2006, Sun et al. named these carbon nanoparticles "carbon quantum dots" (CQDs) and developed a method to make them fluoresce more brightly through surface passivation and chemical modification [2]. CQDs typically exhibit a variety of surface functional groups, including –OH, $–NH_2$, and –COOH, as illustrated in Fig. 1. These functional moieties enhance the versatility of CQDs, allowing for diverse chemical modifications. Their synthesis can be achieved through either top-down or bottom-up approaches. However, the bottom-up method is often preferred due to its higher yield, customisable properties, and the possibility of incorporating heteroatoms by selecting appropriate precursors and synthesis methods [3-4]. Another approach used in CQDs preparation is heteroatom doping, a surface modification method. This technique involves substituting carbon atoms within the sp2/sp3 framework with elements like nitrogen (N), oxygen (O), sulfur (S), or halogens to modify the surface properties of the CQDs [5]. The doping process can be achieved by introducing chemical co-dopants into the precursors during the one-step hydrothermal synthesis of CQDs. This method offers several advantages, including enhanced optical and fluorescence characteristics with high quantum yield (QY), straightforward and cost-efficient synthesis utilising renewable materials, ease of surface modification, as well as non-toxic and highly biocompatible properties [6-7]. In addition, CQDs exhibit outstanding polymerisation capabilities, enabling effective interaction with various biologically active, organic, and inorganic materials [8].

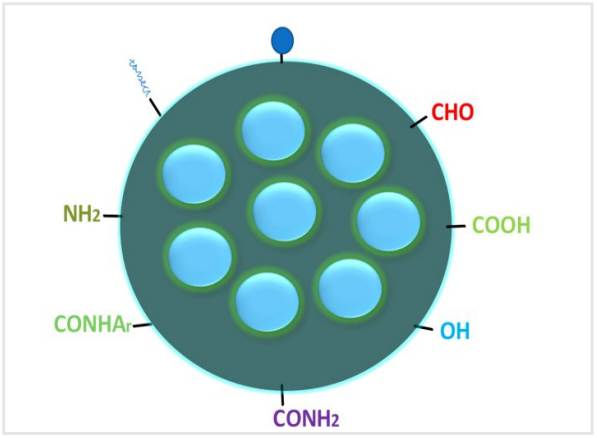

Fig 1 The typical structure of CQDs shows various functional groups (such as carbonyl, carboxyl, hydroxyl, and amino) on their surface [9].

Recently, environmentally friendly carbon precursors have been utilised to explore green production methods, aiming to develop sustainable, cost-efficient, and straightforward techniques. Mahal et al. reported the synthesis of CQDs from oil palm empty fruit bunches (EFB), which exhibited remarkable photoluminescence, water solubility, and stability. These CQDs demonstrated strong absorption at 282 nm, blue fluorescence at 450 nm, and surface hydroxyl and carboxyl groups, making them highly suitable for applications in biomedical fields, energy storage, and water purification [10]. Additionally, Monday et al. synthesised N-doped CQDs using oil palm kernel shells (PKS) for biosensing applications. These CQDs exhibited strong photoluminescence, quantum yields of 13.7 % (CQDs-EDA) and 8.6 % (CQDs-LPh), along with the presence of functional groups such as -OH, -C=O, and $-NH_2$, as confirmed by FTIR and XRD analyses [11]. The utilisation of oil palm waste has predominantly centred on EFB and PKS, leaving oil palm mesocarp fibre (MF) largely underutilised. MF is often incinerated or employed as boiler fuel, contributing to environmental pollution despite its potential as a valuable lignocellulosic resource. With its unique heteroatom composition, including high carbon (46–51.52 wt. %) and oxygen (38–50.21 wt. %) content, MF stands out as an excellent precursor for the targeted synthesis of CQDs, as demonstrated by Onaja et al. and Liew et al [12-13]. In summary, MF contains a significant amount of carbon and oxygen,

https://doi.org/10.24191/esteem.v21iMarch.4713.g3055

making it a highly valuable biomass for diverse industrial applications. Its potential lies particularly in the development of carbon-based materials, with a focus on leveraging green resources derived from MF to synthesise CQDs for efficient CO_2 removal.

Malaysia's CO_2 emissions have surged due to rapid industrialisation, increasing at an average annual rate of 6.12 %. Emissions rose significantly from 14.7 million tonnes in 1972 to 251.6 million tonnes by 2021 [14]. Malaysia targets a 45 % reduction in carbon intensity by 2030, aligning with the IPCC's recommendations for combating climate change through renewable energy adoption and carbon capture storage (CCS) technologies. CCS techniques include liquid absorption, solid material adsorption, and membrane-based separation [15]. Adsorption-based technologies utilising porous solid materials such as activated carbon, zeolite, hydrogel, xerogel, and silica gel are extensively employed as CO_2 adsorbents. These materials are preferred due to their high sorption capacity, large surface area, and substantial pore volume, which enhance the effectiveness of CO_2 capture and storage [16]. The limited adoption of renewable energy in Malaysia underscores the pressing need to advance and promote green technologies, which are crucial for mitigating environmental degradation through sustainable practices and materials.

In this context, CQDs have gained attention as promising materials for CO_2 adsorption due to their adjustable surface functionalities, exceptional chemical stability, and high specific surface area. Incorporating nitrogen and sulfur into the carbon framework of CQDs, combined with chemical activation using KOH, it has proven to enhance the number of adsorption sites optimised for CO_2 removal [17]. Notably, Zaker et al. synthesized N-doped porous carbons from polypyrene (PPy) and KOH, achieving CO_2 adsorption capacities of 7.16, 3.61, and 2.08 mmol/g at 273 K, 303 K, and 333 K, respectively, under 1 bar, demonstrating effectiveness in both dry and humid conditions [18]. For CO2 adsorption, basic nitrogen-containing groups interact selectively with acidic CO_2 via acid-base interactions, thereby enhancing adsorption performance [19]. Sulfur doping has been shown to significantly influence the charge distribution on the carbon surface, thereby enhancing the interaction between the adsorbent and CO_2 molecules [20]. Shi et al. synthesised sulfur-doped carbon using zeolite as a template, achieving a high initial adsorption heat of 59 kJ/mol, which indicates strong interactions between CO_2 and the carbon surface [21]. Although substantial research has been conducted on CO_2 adsorption using carbon doped with a single heteroatom, studies on multi-heteroatom doping, particularly with sulfur (S) and oxygen (O), remain scarce. Co-doping with S and O has been shown to significantly modify the charge distribution on the carbon surface, thereby enhancing interactions with CO_2 molecules. Given that sulfur (S), oxygen (O), and nitrogen (N) each contribute positively to CO_2 uptake, investigating N/S/O co-doped porous carbons for CO_2 capture presents a promising avenue. This study focuses on the synthesis and CO_2 adsorption properties of N/S/O heteroatom-doped CQDs, offering innovative approaches for efficient CO_2 capture.

However, CQDs face stability challenges when synthesised in aqueous media, which can result in aggregation, degradation, and reduction of storage efficiency. These issues adversely affect their performance in solid-state applications such as adsorption and catalysis. To address this, CQDs require a stable support matrix that maintains their intrinsic properties, including surface area, functional groups, and tuneable surface chemistry. Embedding CQDs in xerogels offers a viable solution as xerogels provide a solid and porous matrix for stabilization. Derived from gels, xerogels consist of interconnected particles or polymers that dispersed within a liquid medium, ensuring structural support for the CQDs [22]. The gel undergoes a drying process, such as slow evaporation or freeze-drying, to remove the liquid phase while preserving its overall shape and structure. Although some shrinkage may occur, xerogels retain their high porosity and large surface area, by virtue of the pore network formed during the drying process [23].

Therefore, this study immobilises CQDs into a xerogel matrix using Alias et al.'s methodology to develop an effective CO_2 adsorbent. While CQDs hold significant promise for CO_2 adsorption due to their tuneable surface properties, their instability in aqueous solutions limits their practical use, highlighting the need for stabilization techniques for real-world applications. This research addresses that gap by utilising solid supports like xerogels to stabilise CQDs while preserving their properties across different CQD states, including freeze-dried and various dilution ratios. The variations of CQDs within the xerogel include

https://doi.org/10.24191/esteem.v21iMarch.4713.g3055

dilution ratios of 1:1, 1:10, and 1:50, each influencing the composite's structural integrity and adsorption performance. The innovative combination of CQDs with the porous structure of xerogels enhances CO_2 adsorption, utilising the stability of xerogels and the unique surface chemistry of CQDs for more efficient and selective CO_2 capture.

2. METHODS

2.1 Materials and chemicals

The oil palm mesocarp fibres samples were collected from Taclico Co. Sdn. Bhd., Malaysia. All chemicals were used as received, which are thiourea (99 %, CH_4N_2S), potassium hydroxide (Merck, 30-32 %, KOH), ethanol (R&M Chemical, 96 %, C_2H_6O), glucono-delta-lactone (DChemie, GDL), sodium alginate (R&M Chemical, 91 %), calcium carbonate (R&M Chemical, 99 %, $CaCO_3$), CO_2 gas (AGS Solution) and N_2 gas (AGS Solution).

2.2 Synthesis of mesocarp fibre carbon quantum dots (MF-CQDs)

The synthesis of MF-CQDs involved a modified hydrothermal treatment of the extracted cellulose from oil palm mesocarp fibre (MF). The extracted cellulose of MF followed the method by Syakulu et al [24]. The synthesis of CQDs began by mixing the dried MF cellulose with thiourea and KOH in a ratio of 1:1:3 (MF cellulose: thiourea: KOH). Subsequently, 5.0 g of the developing mixture powder was dissolved in 125 mL of deionised (DI) water and stirred for 30 minutes. This solution was then transferred into a 200 mL Teflon autoclave reactor. The mixture was treated hydrothermally at 180 °C for 24 hours in a universal oven (Memmert GmbH), then allowed to cool to room temperature [25]. As part of the separation process, the suspension and hydrochar were centrifuged at 450 rpm for 10 minutes. The suspension was filtered with a filter membrane to obtain the CQDs aqueous solution for further use.

2.3 Preparation of xerogel-immobilized MF-CQDs (X-MF-CQDs)

The preparation of the X-MF-CQDs method is according to Alias et al [26]. To prepare xerogel-immobilised MF-CQDs, 1 g of sodium alginate was dissolved in 100 ml of distilled water under continuous stirring. Subsequently, 0.2 g of $CaCO_3$, the varying ratio of aqueous MF-CQDs solution and xerogel (1:50, 1:10 and 1:1), and 0.3 g of glucono delta-lactone (GDL) were added in sequence, ensuring complete homogenisation after each addition to form alginate hydrogels. The hydrogel was dried at 60°C for 24 hours in a universal oven (Memmert GmbH). These steps were repeated for freeze-dried MF-CQDs (X-MF-CQDs-FD) to compare the effect of different phases (aqueous and slurry) of CQDs. Table 1 shows the summary of preparation methods and dilution phases for xerogel-immobilised MF-CQDs, highlighting the influence of CQDs concentrations on adsorption performance and structural integrity.

Table 1. Preparation methods and dilution phases of xerogel-immobilised MF-CQDs.

Notation	Description
X-MF-CQDs-FD	Xerogel-immobilised MF-CQDs prepared using freeze-dried CQDs, resulting in a slurry-like phase.
X-MF-CQDs-1:1	Undiluted MF-CQDs directly incorporated into the xerogel matrix (pure form of CQDs).
X-MF-CQDs-1:10	MF-CQDs immobilised at a 1:10 dilution (1-part CQDs to 10 parts xerogel solution).
X-MF-CQDs-1:50	MF-CQDs immobilised at a 1:50 dilution (1-part CQDs to 50 parts xerogel solution)

https://doi.org/10.24191/esteem.v21iMarch.4713.g3055

2.4 Continuous fixed bed adsorption for CO_2 removal

The performance of the CQDs adsorbents was tested in a custom-designed CO_2 adsorption rig, as shown in Fig. 2. A 0.5 g of N/S/O-doped CQDs adsorbents were weighed and placed in the middle of a stainless-steel column and supported with 0.3 g borosilicate glass wool. At ambient temperature, a simulated gas containing CO_2 and N_2 flow passed through the column at 100 mL/min flow rates. The composition of the simulated gas was adjusted by controlling the mass flow meter (Aalborg). The inlet and outlet concentrations of CO_2 were monitored using a portable gas analyser (Optima7 MRU) via a calibrated electrochemical sensor. The concentration of 5 % CO_2 was recorded continuously for every minute, and the adsorption test was stopped until it reached equilibrium (Ci/Co = 0.95). The adsorption capacity of N/S/O-doped CQDs adsorbents was calculated using the adsorption capacity formula as in Eq. (1).

$$q = \frac{Q_f t_f y_f}{m_c} \tag{1}$$

In the equation, q is the adsorption capacity of fresh adsorbent (mg/g), Q_f is the volumetric feed flow rate (mL/min), y_f is the mole fraction of the adsorbate (mg/mL), t_f is the breakthrough time (minute), and m_c is the mass of adsorbent (g).

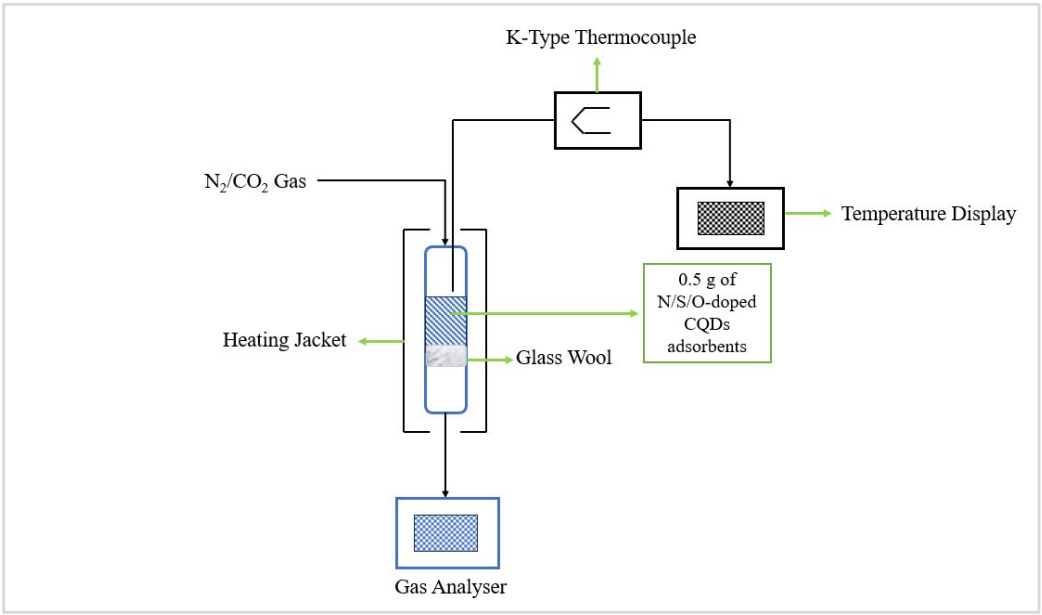

Fig. 2. Schematic diagram of CO_2 adsorption column

2.5 Physical and chemical properties of X-MF-CQDs

The X-MF-CQDs samples were analysed using various characterisation techniques to study its morphology, chemical composition, thermal stability, and porosity. Field Emission Scanning Electron Microscopy coupled with Energy Dispersive X-ray (FESEM-EDX) (Nova NanoSEM 450) was employed to examine the morphology of the X-MF-CQDs samples. The samples were deposited onto carbon tape, and morphological features were observed by analysing three randomly selected xerogels. Elemental analysis was performed using EDX to determine the elemental composition. Fourier Transform Infrared Spectroscopy (FTIR) (Thermo Scientific Nicolet iS10) was used to identify functional groups in the X-MF-CQDs samples by mixing them with KBr at a 1:10 ratio and scanning over a wavelength range of

https://doi.org/10.24191/esteem.v21iMarch.4713.g3055

3500–1000 cm^{-1}. CHNS elemental analysis (Perkin Elmer) was conducted to determine the carbon, hydrogen, nitrogen, and sulfur composition in different dilutions of X-MF-CQDs samples. Finally, thermal stability was evaluated through Thermogravimetric Analysis (TGA) (SDT Q600). 10 mg of the sample from X-MF-CQDs was heated up to 950 °C with a heating rate of 20 °C/min in the presence of air involving a nitrogen atmosphere at 100 ml/min flow rate of gas. Finally, nitrogen adsorption-desorption analysis (model) was performed to assess the porosity, surface area, average pore diameter of X-MF-CQDs samples. The samples were degassed at 120 °C under continuous nitrogen flow of 10 mL/min for 24 hours [27].

3. RESULT AND DISCUSSION

3.1 CO_2 adsorption using X-MF-CQDs adsorbents

Fig. 3 shows the breakthrough curves for CO_2 removal using MF-CQDs and X-MF-CQDs adsorbents at different dilution ratios and freeze-dried conditions. The curves illustrate the relationship between CO_2 concentration at the outlet and adsorption time, highlighting the differences in adsorption performance based on the phase and dilution of the CQDs. All samples have the same operational runtime under the test conditions and a consistent total sorption time of 3600 s to ensure standardisation and comparability of the results. By maintaining a consistent operational runtime, variations in adsorption performance can be attributed solely to differences in material properties, such as surface area, porosity, and functional group availability, rather than differences in test duration. This approach allows for a direct comparison of breakthrough time, adsorption capacity, and overall efficiency between MF-CQDs without xerogel and X-MF-CQDs samples into how dilution ratios and freeze-dried states affect the CO_2 adsorption performance (Table 2).

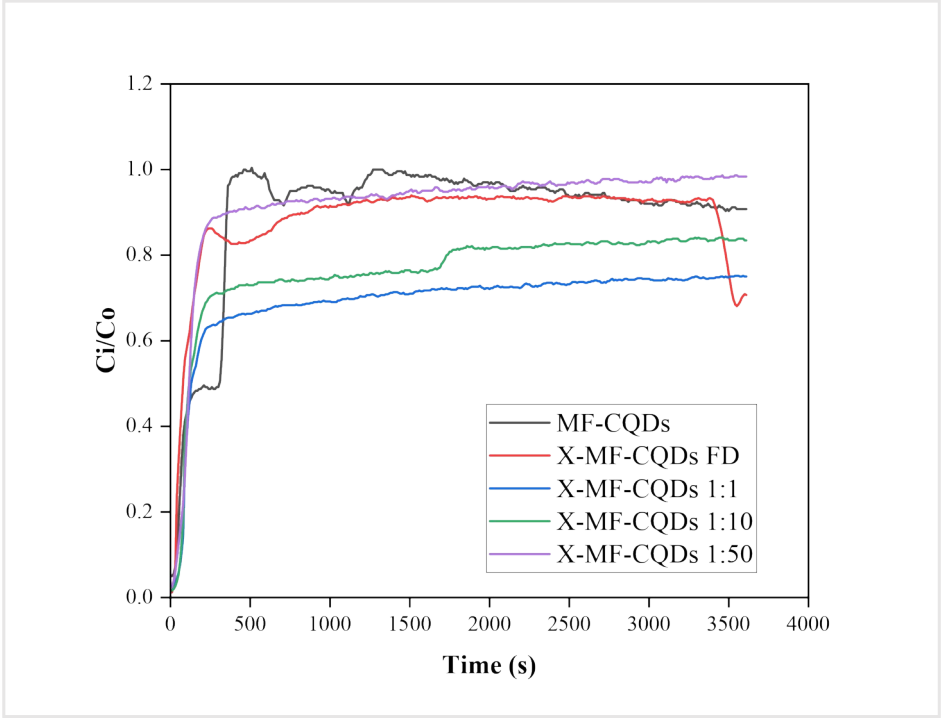

Fig. 3. Breakthrough curve for CO_2 removal using X-MF-CQDs adsorbents

https://doi.org/10.24191/esteem.v21iMarch.4713.g3055

Table 2. CO_2 adsorption performance of X-MF-CQDs adsorbent samples

Sample	Breakthrough Time (s)	Breakthrough Capacity (mg/g)	Total Sorption Capacity (mg/g)
MF-CQDs	39.89	0.3258	12.99
X-MF-CQDs FD	31.94	0.9318	43.67
X-MF-CQD (1:1)	44.17	0.6863	21.81
X-MF-CQDs (1:10)	61.30	0.8637	81.79
X-MF-CQDs (1:50)	46.40	1.0652	129.04

These findings are crucial for tailoring the material's design for specific applications, such as CO_2 capture, and for further optimising its performance through adjustments in synthesis parameters and functionalisation. Among the samples, X-MF-CQDs (1:10) exhibited the longest breakthrough time (61.30 s), indicating it can adsorb CO_2 for an extended period before saturation. This suggests it is effective at trapping and retaining CO_2. The sample also showed a high breakthrough capacity (0.8637 mg/g) and a significant total sorption capacity (81.79 mg/g), reflecting its strong adsorption performance. These improvements are attributed to its well-developed porous structure and the presence of abundant oxygen- and nitrogen-containing functional groups, as confirmed by FTIR analysis. These functional groups enhance CO_2 binding through stronger interactions, such as hydrogen bonding and dipole interactions, improving adsorption efficiency. In comparison, X-MF-CQDs (1:50) achieved the highest breakthrough capacity (1.0652 mg/g) and total sorption capacity (129.04 mg/g), indicating that the 1:50 ratio further optimises adsorption properties. This is likely due to an enhanced balance of porosity, surface area, and functional group availability, which improves gas diffusion and interaction with the active sites. The enhanced adsorption performance of X-MF-CQDs (1:50) can be attributed to its optimised porosity and surface area, as confirmed by BET and HRTEM analysis. However, its slightly shorter breakthrough time (46.40 s) suggests faster saturation, possibly due to rapid adsorption kinetics or slightly lower selectivity for CO_2 retention over time.

The improved performance of X-MF-CQDs (1:10) and X-MF-CQDs (1:50) contrasts with the lower performance of X-MF-CQDs (1:1), which exhibited reduced adsorption capacity due to CQD agglomeration at higher concentrations. Agglomeration reduces the effective surface area and limits the accessibility of adsorption sites, as supported by the lower breakthrough capacity and total sorption capacity of the 1:1 sample. This issue is mitigated in the 1:10 and 1:50 samples, where the xerogel framework prevents agglomeration, ensuring better dispersion of CQDs and improved structural stability. These results highlight the importance of optimising the CQD-to-xerogel ratio to maximize CO_2 capture performance. The 1:10 ratio balances prolonged adsorption duration with high capacity, while the 1:50 ratio achieves the highest capacity, albeit with faster saturation. The X-MF-CQDs FD sample exhibited the shortest breakthrough time of 31.94 s, suggesting rapid CO_2 saturation likely due to structural instability which might be due to its denser structure from freeze-drying, allowing faster initial adsorption. Although it demonstrated a moderate breakthrough capacity of 0.9318 mg/g, its total sorption capacity remained relatively low at 35.44 mg/g. On the other hand, MF-CQDs, which served as the control sample, demonstrated the lowest adsorption performance, with a breakthrough time of 39.89 s, a breakthrough capacity of 0.3258 mg/g, and a total sorption capacity of 12.99 mg/g. This confirms that the xerogel modification significantly enhances CO_2 adsorption efficiency by introducing a more favourable textural and chemical environment for CO_2 binding.

The data in Table 2 also highlights these challenges by showing that MF-CQDs, in their non-xerogel form, exhibit the lowest breakthrough capacity (0.3258 mg/g) and total sorption capacity (12.99 mg/g). This confirms that pristine CQDs have poor CO_2 adsorption performance, likely due to their agglomeration, which reduces porosity and active surface sites available for CO_2 binding. The breakthrough time for MF-

https://doi.org/10.24191/esteem.v21iMarch.4713.g3055

CQDs (39.89 s) is also relatively short, indicating that CO_2 quickly saturates the material, further reinforcing the limitations of CQDs as standalone adsorbents. In contrast, the incorporation of xerogel structures in X-MF-CQDs significantly improves CO_2 adsorption performance by enhancing porosity, preventing particle agglomeration, and providing better structural stability. The X-MF-CQDs (1:10) formulation, for example, demonstrates a much longer breakthrough time (61.30 s), indicating an extended CO_2 adsorption period before saturation. Its breakthrough capacity (0.8637 mg/g) and total sorption capacity (81.79 mg/g) are substantially higher than those of MF-CQDs, showing that the xerogel structure facilitates a more efficient CO_2 capture process. Similarly, X-MF-CQDs (1:50) achieves the highest overall sorption capacity (129.04 mg/g), confirming that the xerogel not only enhances adsorption capacity but also optimises the material's ability to retain CO_2 for longer durations. Furthermore, the breakthrough curve in the provided figure clearly illustrates the difference in adsorption performance between MF-CQDs and xerogel-based samples. The MF-CQDs curve shows an early breakthrough, signifying rapid CO_2 saturation, whereas the X-MF-CQDs samples, particularly the 1:10 and 1:50 formulations, exhibit prolonged breakthrough times and lower Ci/Co values throughout the adsorption process. This trend supports the claim that the xerogel prevents agglomeration and enhances structural stability, leading to a more efficient and sustained CO_2 capture process. The use of xerogel in the synthesis of X-MF-CQDs addresses these limitations by providing a stable, porous framework that prevents agglomeration and enhances structural integrity.

Overall, the X-MF-CQDs (1:50) sample demonstrated the best balance between breakthrough time, capacity, and overall performance, highlighting the importance of controlled CQDs dilution in enhancing CO_2 adsorption. The results emphasise that while higher CQDs concentrations may negatively impact adsorption efficiency, moderate dilution ratios promote better CQDs dispersion and structural stability, optimising the adsorbent's performance for CO_2 capture applications. In summary, the use of xerogel in the synthesis of X-MF-CQDs not only addresses the limitations of agglomeration and structural instability but also significantly enhances the material's CO_2 capture performance. This makes X-MF-CQDs a promising candidate for practical applications in carbon capture and storage.

3.2 Comparison study of X-MF-CQDs and conventional CO_2 adsorbents

CQDs, derived from biomass or other carbon-rich precursors, exhibit unique physicochemical characteristics that enhance CO_2 adsorption through mechanisms such as π–π interactions and heteroatom doping. Similarly, xerogels, with their porous and lightweight structure, offer high gas adsorption capacities and can serve as effective supports for CQDs to mitigate their agglomeration issues. While studies have reported CO_2 adsorption capacities of CQDs and xerogel-based materials under various conditions, a direct comparison with conventional adsorbents such as activated carbon, metal-organic frameworks (MOFs), zeolites, and amine-modified materials are essential to evaluate their feasibility for large-scale applications. This study aims to set a benchmark for CO_2 adsorption performance of CQDs and xerogel-based hybrid materials against these conventional adsorbents, providing a comprehensive analysis of their potential in CO_2 capture technologies.

Based on Table 3, the CO_2 adsorption performance of X-MF-CQDs (1:50) is compared against other established adsorbents, including activated carbon, MOF-based adsorbents, and carbon nanoparticle-based adsorbents, to benchmark its effectiveness. The X-MF-CQDs (1:50) exhibited an adsorption capacity of 129.04 mg/g, positioning it within the higher range of conventional adsorbents. Activated carbon, a widely used porous material for CO_2 capture, typically demonstrates an adsorption capacity between 50-150 mg/g [28]. The performance of X-MF-CQDs (1:50) surpasses the lower-end values of activated carbon and aligns closely with its upper range, suggesting that xerogel-modified CQDs can compete with traditional carbon-based adsorbents. MOF-based adsorbents, known for their tuneable pore structures and high surface areas, generally exhibit adsorption capacities between 100-300 mg/g [29]. Although some MOFs outperform X-MF-CQDs (1:50), certain MOF variants fall within the same adsorption range. This comparison highlights the efficiency of xerogel-enhanced CQDs while also acknowledging that further

https://doi.org/10.24191/esteem.v21iMarch.4713.g3055

optimisation, such as functionalisation or structural modifications, could enhance their adsorption performance further. Carbon nanoparticle-based adsorbents, on the other hand, demonstrate relatively lower CO_2 adsorption capacities, ranging from 20-50 mg/g [30]. The significantly higher performance of X-MF-CQDs (1:50) compared to carbon nanoparticles underscores the advantage of incorporating a xerogel matrix. Xerogels provide a structured, porous framework that mitigates CQD agglomeration, leading to more accessible adsorption sites and enhanced CO_2 capture efficiency. These comparisons validate the potential of X-MF-CQDs (1:50) as a promising alternative to conventional adsorbents. While it performs competitively with activated carbon and MOF-based adsorbents, it significantly outperforms carbon nanoparticle-based materials. The findings support the notion that hybridising CQDs with xerogels effectively addresses the limitations of CQDs alone, such as agglomeration and structural instability, thereby enhancing CO_2 adsorption performance.

Table 3 Previous studies of conventional CO_2 adsorbent

Adsorbent	Adsorption Capacity (mg/g)	Reference
X-MF-CQDs (1:50)	129.04	This Study
Activated Carbon	50-150	Acevedo et. Al 2020
MOF-based Adsorbent	100-300	Mahajan et al., 2022
Carbon nanoparticles-based Adsorbent	20-50	Dziejarski et al., 2023

3.3 Surface functional groups of X-MF-CQDs

The FTIR spectrum in Fig. 4., displays the transmittance intensities of various functional groups in X-MF-CQDs FD and X-MF-CQDs at different dilution chemical loading ratios (1:1, 1:10, and 1:50). The strong broadband peaks at 3440 cm $^{-1}$ corresponds to the N–H functional groups, and the vibration peak of C=N was discovered at 1643 cm $^{-1}$, highlighting that the nitrogen-containing group was successfully doped on CQDs' surface [31]. The FTIR spectra also reveals that the N-H and C=N stretching peaks were more pronounced in the freeze-dried (FD) and low-dilution (1:1) samples. At the same time, their intensities decreased with higher dilution (1:50). This suggests that excess nitrogen doping leads to abundant amine (N-H) and imine (C=N) groups at lower dilution ratios. The high concentration of these functional groups promotes hydrogen bonding and excessive cross-linking, which can disrupt the formation of a robust and porous xerogel network.

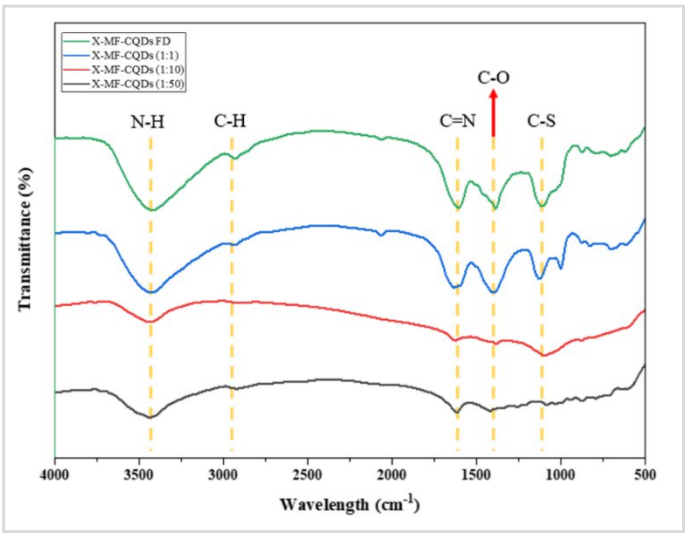

Fig. 4. FTIR spectroscopy of X-MF-CQDs samples

https://doi.org/10.24191/esteem.v21iMarch.4713.g3055

A study by Principe and Fletcher demonstrated that the incorporation of nitrogen-rich materials into xerogels enhances CO_2 selectivity, as observed in melamine-resorcinol-formaldehyde xerogels [32]. Jeon et al. also found that while nitrogen doping reduces the specific surface area and micropore volume, it introduces basic sites that enhance CO_2 selectivity [33]. Next, the 1400 cm^{-1} and 1277 cm^{-1} peaks can be attributed to the C-O and C-S functional groups, respectively, comparable to a study conducted by Aygun et al. [34]. At higher dilution (1:50), the reduced intensities of C=O and C=S suggest lower levels of functional group saturation, resulting in a more stable xerogel structure. This balance minimises excessive cross-linking and aggregation, promoting the formation of a solid adsorbent with improved structural integrity. All FTIR data successfully demonstrated the formation of N/S/O-doped CQDs, which is necessary as a promising adsorbent candidate for CO_2 capture applications. As stated by Zhu et al., the presence of specific functional groups can also promote chemical interactions with CO_2, leading to higher adsorption capacities [35]. The FTIR peak intensities show clear trends, with X-MF-CQDs FD having the most substantial peaks across all functional groups. As the chemical loading ratio decreases from 1:1 to 1:10 and 1:50, peak intensities also decrease. However, the material takes on a slurry-like texture at lower dilution ratios and freeze-dried conditions, which may weaken the network and reduce stability, limiting its effectiveness as a solid CO_2 adsorbent. This trend suggests a decrease in surface functional groups that maintain the xerogel's structure.

3.4 Thermal stability of X-MF-CQDs

The provided TGA analysis evaluates the thermal stability and decomposition behaviour of the X-MF-CQDs samples with varying dilutions, as shown in Fig. 5. The following key observations can be made regarding the thermal profiles of the sample.

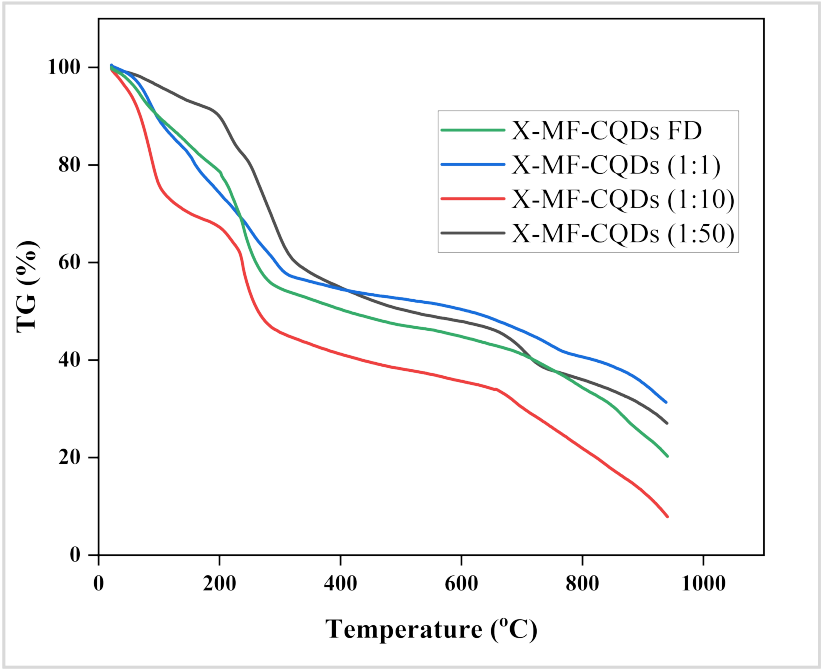

Fig. 5. Thermal stability of X-MF-CQDs samples

https://doi.org/10.24191/esteem.v21iMarch.4713.g3055

The first section represents the first moisture degradation, the second section describes the volatile matter decomposition, and the last section is the fixed carbon, where they were referring to the distinct phases observed in the Thermogravimetric Analysis (TGA) curve of the X-MF-CQDs [36]. These phases represent the different stages of material decomposition as the temperature increases. All samples show a slight initial weight loss at temperatures below 150 °C in the first section (moisture degradation), which is attributed to the evaporation of adsorbed moisture and volatile compounds [37]. This is a common observation in porous or gel-based materials, as water molecules or low molecular weight species are typically retained within the structure. The significant weight loss observed between 150 °C and 600 °C in second section (volatile matter decomposition) corresponds to the thermal decomposition of organic components, particularly CQDs and MF content [38]. This region reflects the pyrolysis of carbon-containing materials, and the breakdown of the heteroatoms (N/S/O doping) incorporated into the X-MF-CQDs structure. The red curve (X-MF-CQDs (1:1)) shows the highest weight loss in this region, indicating a higher proportion of organic or less thermally stable material. This could be due to the higher CQDs concentration, which may hinder strong bonding or stabilisation within the xerogel structure. The black curve (X-MF-CQDs (1:50)) demonstrates the lowest weight loss, suggesting more excellent thermal stability due to a lower CQDs content and more robust stabilisation within the xerogel network. The curves stabilise at temperatures above 600°C in the last section (fixed carbon), and minimal weight loss is observed, indicating that the remaining material consists of thermally stable carbonaceous residues (char or graphitised carbon). As the dilution decreases (higher CQDs concentration), the material's thermal stability decreases, as evident from the larger weight losses and lower residual weights. This can be attributed to the overloading of CQDs, which disrupts the stable xerogel network, resulting in a less thermally robust material. X-MF-CQDs FD sample (green curve) shows moderate thermal stability, suggesting that freeze-drying improves the initial structural stability but may not eliminate moisture or weakly bound volatile components. Finally, TGA analysis shows that lower CQDs dilution ratios (1:1) resulted in reduced thermal stability due to structural disruption and higher organic content. In contrast, higher dilution ratios (1:50) improve thermal stability, making them more suitable for mild temperature applications like CO_2 adsorption.

3.5 Surface characteristic of X-MF-CQDs

The FESEM analysis provides the morphology and structural characteristics of the X-MF-CQDs samples, as shown in Fig. 6, at 100x and 10kx magnification levels.

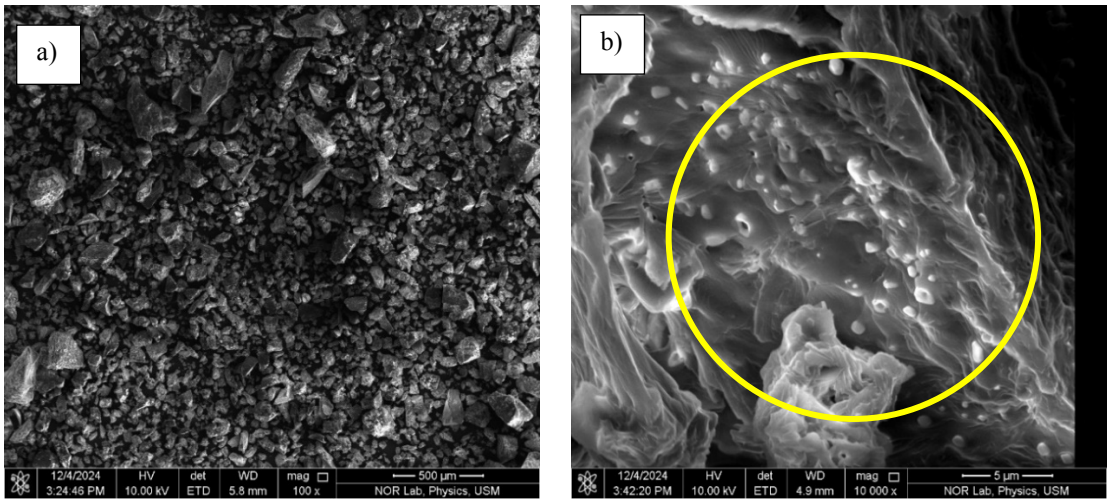

Fig. 6. FESEM micrograph of X-MF-CQDs (1:50) sample at 100x and 10kx magnification level, (a) overall distribution of X-MF-CQDs and (b) microporous structure of X-MF-CQDs

https://doi.org/10.24191/esteem.v21iMarch.4713.g3055

Based on Fig. 6. (a), the micrographs revealed the overall distribution of xerogel-immobilised on CQDs derived MF surface, indicating a relatively uniform coating and well-dispersed CQDs within the xerogel matrix after immobilisation. However, slight agglomeration or clustering of particles may be observed, depending on the dilution ratios used during the preparation process. The surface of the X-MF-CQDs was brittle due to the properties of xerogel being highly dependent on the solid component and the bulk density. Fig. 6. (b) shows most of the MF-CQDs were immersed in the alginate surface, which preserved its form and had pores that have potential as an adsorbent material. The FESEM image of X-MF-CQDs at 10kx magnification, highlighting the microporous structure (circled) as this porous network is particularly important for facilitating CO_2 adsorption due to its high surface area and enhanced accessibility for gas molecules. The porosity observed in the structure supports the role of xerogel as a stabilising platform for MF-CQDs, allowing for their effective immobilisation. Furthermore, the distribution of MF-CQDs on the xerogel surface appears critical, as a homogeneous dispersion is expected to maximize the adsorption capacity by exposing more active sites. The EDX spectra further validated the elemental composition of X-MF-CQDs, which predominantly consisted of carbon (50.33 wt. %), oxygen (22.78 wt. %), sulfur (0.6 wt. %), potassium (2.83 wt. %) during synthesis of MF-CQDs. The presence of calcium (5.76 wt. %) and sodium (5.32 wt. %) in the EDX spectra is attributed to the xerogel immobilisation process of MF-CQDs (Table 3). These elements originate from the key reagents used during the preparation of the xerogel.

Table 3. EDX composition of X-MF-CQDs

Sample	Carbon, wt. %	Oxygen, wt. %	Sulfur, wt. %	Potassium, wt. %	Sodium, wt. %	Calcium, wt. %
X-MF-CQDs (1:50)	50.33	22.78	0.6	2.83	5.32	5.76

3.6 Elemental analysis of X-MF-CQDs

The CHNS elemental analysis of the synthesised materials X-MF-CQDs 1:50 and X-MF-CQDs 1:50 spent highlight the chemical composition and structural changes occurring during the synthesis and adsorption processes (Table 4). This analysis shows the influence of carbon (C), hydrogen (H), nitrogen (N), sulfur (S), and other residual elements, such as oxygen and ash, on the properties of the X-MF-CQDs. Comparing the fresh and spent samples reveals how the material evolves during use, particularly in terms of its elemental composition.

Table 4. Elemental composition of X-MF-CQDs

Sample	Carbon, wt. %	Hydrogen, wt. %	Nitrogen, wt. %	Sulfur, wt. %
X-MF-CQDs 1:50	26.83	4.72	0.52	0.99
X-MF-CQDs 1:50 Spent	23.69	4.09	0.46	0.82

The comparison between the X-MF-CQDs 1:50 fresh sample and the X-MF-CQDs 1:50 spent sample, as revealed by CHNS elemental analysis of material's structural and chemical changes during the adsorption process. The fresh sample exhibits a carbon content of 26.83 wt. %, indicating a carbon-rich structure derived from MF, along with hydrogen (4.72 wt. %), nitrogen (0.52 wt. %), and sulfur (0.99 wt. %) content, suggesting successful doping with heteroatoms. These heteroatoms, particularly nitrogen and sulfur, introduce polar functional groups that enhance the material's adsorption properties by providing basic and reactive sites for CO_2 interaction. However, after being used in the adsorption process, the spent sample

https://doi.org/10.24191/esteem.v21iMarch.4713.g3055

shows a reduction in all elemental contents: carbon decreases to 23.69 wt. %, hydrogen to 4.09 wt. %, nitrogen to 0.46 wt. %, and sulfur to 0.82 wt. %. This reduction in carbon content suggests partial degradation of the carbon framework, possibly due to oxidation or structural breakdown during the adsorption process. The decrease in hydrogen content indicates the potential loss of hydroxyl or aliphatic groups, which could affect the material's hydrophilicity and interaction with CO_2. Similarly, the reduction in nitrogen and sulfur content implies that some of the functional groups responsible for CO_2 adsorption such as amines group may have been consumed or altered during the adsorption process. The findings underscore the importance of optimising the material's composition and developing effective regeneration strategies to restore its adsorption performance over multiple cycles for further studies.

3.7 Pore size distribution of X-MF-CQDs and its surface properties

The structural characteristics of an adsorbent, including surface area and pore size distribution play a crucial role in determining its CO_2 adsorption performance. The BET analysis in Fig. 7 and Table 5 provide in depth understanding into the specific surface area and pore size distribution, which are critical factors influencing gas adsorption capacity and kinetics. Furthermore, HRTEM analysis in Fig. 8 complements the BET findings by providing direct visualisation of the material's porous structure. The HRTEM micrographs reveal CQDs embedded within the xerogel matrix, with a distinct contrast between the dark carbon-rich quantum dots and the surrounding lighter xerogel network.

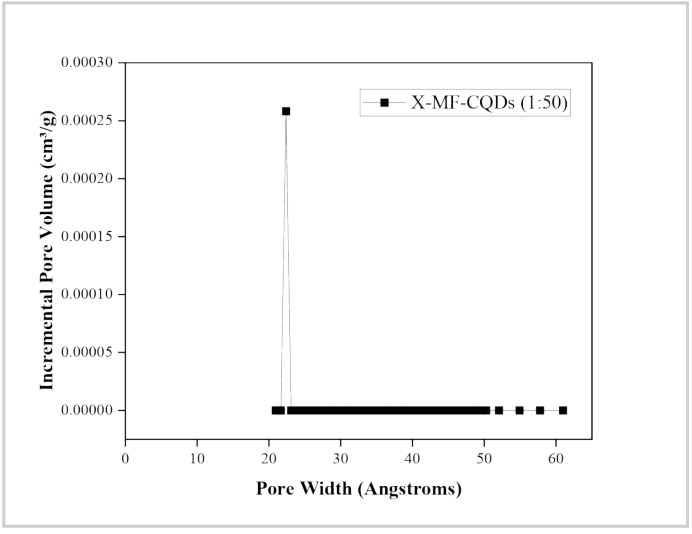

Fig. 7. The pore size distribution of X-MF-CQDs (1:50) sample

Table 5. Surface area of X-MF-CQDs (1:50) sample

Sample	BET surface area, m^2/g
X-MF-CQDs (1:50)	0.7011

As presented in the Fig. 7, the pore size distribution of X-MF-CQDs (1:50) demonstrates a dominant peak around ~20 Å (2 nm) indicating a primarily microporous structure. Micropores play a crucial role in CO_2 adsorption due to their comparable size to CO_2 molecules (3.3 Å), promoting strong physisorption interactions via van der Waals forces [39]. However, the presence of a minor broad peak beyond 50 Å (5 nm and above) suggests a small fraction of mesopores. Mesopores contribute to facilitating gas diffusion into micropores, improving accessibility and adsorption kinetics. While micropores enhance CO_2 capture due to confinement effects, excessive micro porosity without mesopores can lead to diffusion limitations,

https://doi.org/10.24191/esteem.v21iMarch.4713.g3055

potentially reducing adsorption rates [40]. However, the BET surface area of X-MF-CQDs (1:50) is relatively low (0.7011 m^2/g), indicating that the material does not rely on extensive surface area for CO_2 capture but rather on pore structure and surface functionalisation. The presence of heteroatoms (N, S, O) within the xerogel matrix, as observed in FTIR, EDX and elemental analysis, enhances CO_2 affinity by introducing sites for chemisorption and dipole–quadrupole interactions [41]. The micropore-dominated structure of X-MF-CQDs aligns with its high CO_2 adsorption capacity (129.04 mg/g), as micropores provide strong confinement effects for gas molecules. The minimal mesoporosity suggests that the material might experience some limitations in adsorption kinetics, but this is compensated by the presence of surface functional groups that enhance CO_2 affinity.

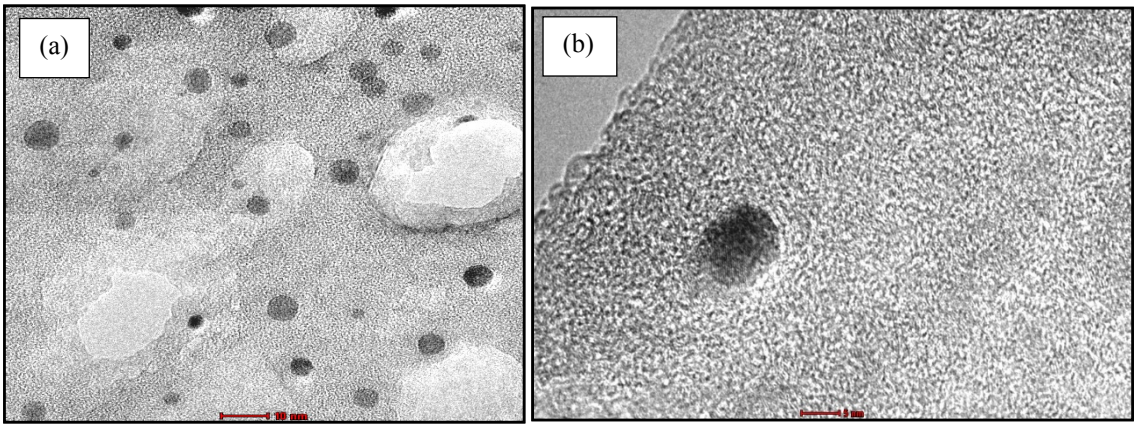

Fig. 8. HRTEM micrograph of X-MF-CQDs (1:50) sample at 10 nm and 15 nm magnification level, (a) overall distribution of X-MF-CQDs and (b) microporous structure of X-MF-CQDs

Compared to conventional adsorbents such as MOFs (100–300 mg/g) and activated carbon (50–150 mg/g)**,** the X-MF-CQDs system achieves competitive adsorption performance despite its low surface area, highlighting the role of pore structure and functionalisation in determining adsorption efficiency [42-43]. A study by Vivo-Vilches et al. highlights that high porosity plays a key role in gas adsorption by increasing the number of available adsorption sites, resulting in greater CO_2 uptake. For example, carbon xerogel achieved a CO_2 uptake of 6.57 mol/kg, attributed to its extensive micropore volume [44]. The synergy between micro porosity, functional group interactions, and structural stability contributes to its high adsorption efficiency, validating its potential as a promising adsorbent for CO_2 capture applications**.** The HRTEM micrograph in Fig. 8 further supports the microporous nature of X-MF-CQDs by revealing the presence of nanostructured CQDs embedded within the xerogel matrix**.** The dark regions observed in the HRTEM images correspond to the highly dense CQDs, while the lighter areas represent the surrounding xerogel structure. Additionally, the uniform dispersion of CQDs in the xerogel is crucial in maintaining a stable porous network. This structure prevents pore collapse and ensures that CO_2 molecules can efficiently access the micropores. The interconnected porous framework is expected to facilitate gas diffusion while ensuring a high density of adsorption sites, which directly influences the breakthrough time and total sorption capacity. In the X-MF-CQDs samples, the xerogel matrix acts as a structural stabiliser that disperses the CQDs uniformly, preventing their excessive agglomeration while maintaining its porosity.

4. CONCLUSIONS

In conclusion, this study highlights the promising potential of xerogel-immobilised carbon quantum dots (X-MF-CQDs) derived from oil palm mesocarp fibre (MF) as a sustainable and effective material for CO_2

https://doi.org/10.24191/esteem.v21iMarch.4713.g3055

adsorption. Through hydrothermal synthesis, oil palm waste was successfully transformed into high-value CQDs, with the incorporation of functional groups significantly enhancing their adsorption properties. The optimised synthesis using a 1:3:3 ratio of cellulose, thiourea, and potassium hydroxide (KOH) produced MF-derived CQDs with improved surface functionalities, including carboxyl, hydroxyl, amino, and sulfur groups, as confirmed by FTIR analysis. The use of xerogel immobilisation further improved the stability and CO_2 adsorption efficiency of the material. The X-MF-CQDs demonstrated optimal CO_2 capture at a 1:50 dilution (129.04 mg/g), emphasising the importance of proper CQD dispersion and structural integrity. Despite a relatively low BET surface area (0.7011 m^2/g), the high adsorption performance suggests that micropore-dominated adsorption and functional group interactions play a crucial role in CO_2 capture. Pore size distribution analysis revealed a dominant peak at ~20 Å (2 nm), confirming the presence of micropores, which are particularly effective for CO_2 adsorption due to their comparable size to CO_2 molecules (~3.3 Å). The presence of minor mesopores further supports gas diffusion and accessibility to active adsorption sites, optimising adsorption kinetics. HRTEM analysis confirmed that the CQDs were embedded within the xerogel matrix, providing enhanced stability and dispersion, which minimised agglomeration issues often associated with CQDs. This structural arrangement effectively facilitated gas diffusion and interaction with active adsorption sites, further validating the role of xerogel in overcoming the limitations of conventional CQDs. Additionally, TGA analysis revealed that higher CQDs's concentrations (1:1) reduced thermal stability, while lower concentrations (1:50) improved it, offering a more stable structure. FESEM micrographs also confirmed a uniform distribution of CQDs within the xerogel matrix, essential for adsorption. The elemental composition, with carbon (50.33%), oxygen (22.78%), and sulfur (0.6%), supports the role of heteroatoms in enhancing CO_2 adsorption. These findings highlight the synergistic effect of microporous structure, heteroatom doping, and xerogel stabilisation in optimizing CO_2 capture, demonstrating the potential of oil palm waste valorisation for sustainable environmental applications.

5. ACKNOWLEDGEMENTS/FUNDING

The authors would like to acknowledge the support of the Ministry of Higher Education (MOHE), Malaysia, through the Fundamental Research Grant Scheme (Grant No. FRGS/1/2022/TK0/UITM/02/55). The authors are grateful for the facilities provided by Universiti Teknologi MARA (UiTM) Cawangan Pulau Pinang for providing the facilities and financial support for this research.

6. CONFLICT OF INTEREST STATEMENT

The authors agree that this research was conducted without any self-benefits, commercial or financial conflicts and declare the absence of conflicting interests with the funders.

7. AUTHORS' CONTRIBUTIONS

Aimi Solihah Zaul Kapri: Conceptualisation, methodology, formal analysis, investigation and writing-original draft; **Norhusna Mohamad Nor**: Conceptualisation, methodology, formal analysis, supervision, writing- review and editing, and validation.

8. REFERENCES

[1] L. Cui, X. Ren, M. Sun, H. Liu, and L. Xia, "Carbon dots: Synthesis, properties and applications," *Nanomaterials*, vol. 11, no. 12, Dec. 2021. Available: https://doi.org/10.3390/nano11123419

[2] T. C. Wareing, P. Gentile, and A. N. Phan, "Biomass-Based Carbon Dots: Current Development and Future Perspectives," *ACS Nano*, vol. 15, no. 10, pp. 15471–15501, 2021. Available:

https://doi.org/10.1021/acsnano.1c03886

[3] S. Dinç, M. Kara, A. Ve, D. Dergisi, and S. Dinc, "Synthesis and Applications of Carbon Dots from Food and Natural Products: A Mini-Review," 2018. [Online]. Available: www.dergipark.gov.tr/jan

[4] S. Li et al., "The development of carbon dots: From the perspective of materials chemistry," *Materials Today*, vol. 51, no. December, pp. 188–207, 2021. Available: https://doi.org/10.1016/j.mattod.2021.07.028

[5] S. Sagbas and N. Sahiner, "Carbon dots: Preparation, properties, and application," in *Nanocarbon and its Composites: Preparation, Properties and Applications*, Elsevier, 2018, pp. 651–676. Available: https://doi.org/10.1016/B978-0-08-102509-3.00022-5

[6] S. Das, L. Ngashangva, and P. Goswami, "Carbon dots: An emerging smart material for analytical applications," *Micromachines (Basel)*, vol. 12, no. 1, pp. 1–36, Jan. 2021. Available: https://doi.org/10.3390/MI12010084

[7] S. Das, L. Ngashangva, and P. Goswami, "Carbon dots: An emerging smart material for analytical applications," *Micromachines (Basel)*, vol. 12, no. 1, pp. 1–36, Jan. 2021, doi: 10.3390/MI12010084.

[8] S. E. Elugoke, G. E. Uwaya, T. W. Quadri, and E. E. Ebenso, "Carbon Quantum Dots: Basics, Properties, and Fundamentals," in *ACS Symposium Series*, vol. 1465, American Chemical Society, 2024, pp. 3–42. Available: https://doi.org/10.1021/bk-2024-1465.ch001

[9] P. K. Yadav, S. Chandra, V. Kumar, D. Kumar, and S. H. Hasan, "Carbon Quantum Dots: Synthesis, Structure, Properties, and Catalytic Applications for Organic Synthesis," *Catalysts*, vol. 13, no. 2, Feb. 2023. Available: https://doi.org/10.3390/catal13020422

[10] N. A. Mahat and S. A. Shamsudin, "Blue luminescence carbon quantum dots derived from oil palm empty fruit bunch biomass," in *IOP Conference Series: Materials Science and Engineering*, Institute of Physics Publishing, Mar. 2020. Available: https://doi.org/10.1088/1757-899X/736/5/052001, doi: 10.1088/1757-899X/736/5/052001

[11] Y. N. Monday, J. Abdullah, N. A. Yusof, S. A. Rashid, and R. H. Shueb, "Facile hydrothermal and solvothermal synthesis and characterization of nitrogen-doped carbon dots from palm kernel shell precursor," *Applied Sciences*, vol. 11, no. 4, Feb. 2021. Available: https://doi.org/10.3390/app11041630, doi: 10.3390/app11041630

[12] E. Onoja, S. Chandren, F. I. Abdul Razak, N. A. Mahat, and R. A. Wahab, "Oil Palm (Elaeis guineensis) Biomass in Malaysia: The Present and Future Prospects," *Springer Netherlands*, Aug. 1, 2019. Available: https://doi.org/10.1007/s12649-018-0258-1

[13] R. K. Liew et al., "Oil palm waste: An abundant and promising feedstock for microwave pyrolysis conversion into good quality biochar with potential multi-applications," *Process Safety and Environmental Protection*, vol. 115, pp. 57–69, Apr. 2018. Available: https://doi.org/10.1016/j.psep.2017.10.005

[14] S. S. Shamsul Azlan, N. R. Abd Rahman, and M. Mohamad, "Carbon Emission in Malaysia: Trends and Initiatives of Government," *International Journal of Academic Research in Accounting, Finance and Management Sciences*, vol. 13, no. 1, Feb. 2023. Available: https://doi.org/10.6007/ijarafms/v13-i1/15879

[15] J. Xu, K. G. Haw, Z. Li, S. Pati, Z. Wang, and S. Kawi, "A mini-review on recent developments in SAPO-34 zeolite membranes and membrane reactors," *React Chem Eng*, vol. 6, no. 1, pp. 52–66, Jan. 2021. Available: https://doi.org/10.1039/D0RE00349B

[16] X. Y. D. Soo et al., "Advancements in CO2 capture by absorption and adsorption: A comprehensive review," *Journal of CO2 Utilization*, vol. 70, p. 102727, Mar. 2024. Available: https://doi.org/10.1016/j.jcou.2024.102727

[17] Y. Zhou, P. Tan, Z. He, C. Zhang, Q. Fang, and G. Chen, "CO2 adsorption performance of nitrogen-doped porous carbon derived from licorice residue by hydrothermal treatment," *Fuel*, vol. 311, p. 122507, 2022. Available: https://doi.org/10.1016/j.fuel.2021.122507

[18] A. Zaker, S. ben Hammouda, J. Sun, X. Wang, X. Li, and Z. Chen, "Carbon-based materials for CO_2 capture: Their production, modification and performance," *J. Environ. Chem. Eng.*, vol. 11, no. 5, Jun. 2023. Available: https://doi.org/10.1016/j.jece.2023.109741

[19] Q. Li, S. Liu, L. Wang, F. Chen, J. Shao, and X. Hu, "Efficient nitrogen doped porous carbonaceous CO_2 adsorbents based on lotus leaf," *J. Environ. Sci. (China)*, vol. 103, pp. 268–278, May 2021. Available:

https://doi.org/10.24191/esteem.v21iMarch.4713.g3055

https://doi.org/10.1016/j.jes.2020.11.008
[20] C. Ma, T. Lu, J. Shao, J. Huang, X. Hu, and L. Wang, "Biomass derived nitrogen and sulfur co-doped porous carbons for efficient CO_2 adsorption," *Sep. Purif. Technol.*, vol. 281, Jan. 2022. Available: https://doi.org/10.1016/j.seppur.2021.119899
[21] J. Shi, H. Cui, J. Xu, N. Yan, C. Zhang, and S. You, "Synthesis of nitrogen and sulfur co-doped carbons with chemical blowing method for CO_2 adsorption," *Fuel*, vol. 305, Dec. 2021. Available: https://doi.org/10.1016/j.fuel.2021.121505
[22] A. K. Nayak and B. Das, "Introduction to polymeric gels," in *Polymeric Gels*, Elsevier, 2018, pp. 3–27. Available: https://doi.org/10.1016/b978-0-08-102179-8.00001-6
[23] S. Yamasaki *et al.*, "Nanocellulose xerogels with high porosities and large specific surface areas," *Front. Chem.*, vol. 7, no. MAY, 2019. Available: https://doi.org/10.3389/fchem.2019.00316
[24] N. F. Sayakulu and S. Soloi, "The effect of sodium hydroxide (NaOH) concentration on oil palm empty fruit bunch (OPEFB) cellulose yield," in *J. Phys.: Conf. Ser.*, Institute of Physics, 2022. Available: https://doi.org/10.1088/1742-6596/2314/1/012017
[25] H. Zhou, Y. Ren, Z. Li, W. He, and Z. Li, "Selective detection of Fe^{3+} by nitrogen–sulfur-doped carbon dots using thiourea and citric acid," *Coatings*, vol. 12, no. 8, 2022. Available: https://doi.org/10.3390/coatings12081042
[26] A. B. Alias, D. Qarizada, N. S. A. Malik, N. M. R. Noraini, and Z. A. Rashid, "Comparison of hydrogel- and xerogel-based sorbent from empty fruit bunch (EFB)," *Arch. Mater. Sci. Eng.*, vol. 118, no. 2, pp. 49–60, Dec. 2022. Available: https://doi.org/10.5604/01.3001.0016.2579
[27] N. M. R. Noraini, A. B. Alias, D. Qarizada, F. A. M. Azman, Z. A. Rashid, and M. R. C. Hasan, "Synthesis and characterization of xerogel from palm kernel shell biochar," *J. Mech. Eng.*, vol. 11, no. Special Issue 1, pp. 211–226, 2022. Available: https://doi.org/10.24191/jmeche.v11i1.23599
[28] S. Acevedo, L. Giraldo, and J. C. Moreno-Piraján, "Adsorption of CO_2 on activated carbons prepared by chemical activation with cupric nitrate," *ACS Omega*, vol. 5, no. 18, pp. 10423–10432, May 2020. Available: https://doi.org/10.1021/acsomega.0c00342
[29] S. Mahajan and M. Lahtinen, "Recent progress in metal-organic frameworks (MOFs) for CO_2 capture at different pressures," *J. Environ. Chem. Eng.*, vol. 10, no. 6, p. 108930, Dec. 2022. Available: https://doi.org/10.1016/j.jece.2022.108930
[30] B. Dziejarski, J. Serafin, K. Andersson, and R. Krzyżyńska, "CO_2 capture materials: A review of current trends and future challenges," *Mater. Today Sustain.*, vol. 24, p. 100483, Dec. 2023. Available: https://doi.org/10.1016/j.mtsust.2023.100483
[31] M. A. Mousa, H. H. Abdelrahman, M. A. Fahmy, D. G. Ebrahim, and A. H. E. Moustafa, "Pure and doped carbon quantum dots as fluorescent probes for the detection of phenol compounds and antibiotics in aquariums," *Sci. Rep.*, vol. 13, no. 1, Dec. 2023. Available: https://doi.org/10.1038/s41598-023-39490-y
[32] I. A. Principe and A. J. Fletcher, "Adsorption selectivity of CO_2 over CH_4, N_2 and H_2 in melamine–resorcinol–formaldehyde xerogels," *Adsorption*, vol. 26, no. 5, pp. 723–735, Jul. 2020. Available: https://doi.org/10.1007/s10450-020-00203-w
[33] D. H. Jeon, B. G. Min, J. G. Oh, C. Nah, and S. J. Park, "Influence of nitrogen moieties on CO_2 capture of carbon aerogel," *Carbon Lett.*, vol. 16, no. 1, pp. 57–61, Jan. 2015. Available: https://doi.org/10.5714/cl.2015.16.1.057
[34] A. Aygun, I. Cobas, R. N. E. Tiri, and F. Sen, "Hydrothermal synthesis of B, S, and N-doped carbon quantum dots for colorimetric sensing of heavy metal ions," *RSC Adv.*, vol. 14, no. 16, pp. 10814–10825, Apr. 2024. Available: https://doi.org/10.1039/d4ra00397g
[35] Q. Zhu *et al.*, "Highly porous carbon xerogels doped with cuprous chloride for effective CO adsorption," *ACS Omega*, vol. 4, no. 4, pp. 6138–6143, Apr. 2019. Available: https://doi.org/10.1021/acsomega.8b03647
[36] A. B. Alias, D. Qarizada, N. S. A. Malik, N. M. R. Noraini, and Z. A. Rashid, "Comparison of hydrogel- and xerogel-based sorbent from empty fruit bunch (EFB)," *Arch. Mater. Sci. Eng.*, vol. 118, no. 2, pp. 49–60, Dec. 2022. Available: https://doi.org/10.5604/01.3001.0016.2579
[37] G. Güzel Kaya, "Polyethylene glycol/silica and carbon black/silica xerogel composites as an adsorbent

for CO_2 capture," *Turk. J. Chem.*, vol. 45, no. 6, pp. 2013–2023, 2021. Available: https://doi.org/10.3906/kim-2101-45

[38] A. Kechagias *et al.*, "Development and characterization of N/S-carbon quantum dots by valorizing Greek crayfish food waste," *Appl. Sci. (Switz.)*, vol. 13, no. 15, Aug. 2023. Available: https://doi.org/10.3390/app13158730

[39] H. Cai, L. Fu, H. Pan, Z. Yan, T. Chen, and T. Zhao, "Pore engineering of ultramicroporous carbon from an N-doped polymer for CO_2 adsorption and conversion," *Mol. Catal.*, vol. 550, Nov. 2023. Available: https://doi.org/10.1016/j.mcat.2023.113557

[40] W. Shi, J. Yu, H. Liu, D. Gao, A. Yuan, and B. Chang, "Hierarchically nanoporous carbon for CO_2 capture and separation: Roles of morphology, porosity, and surface chemistry," *ACS Appl. Nano Mater.*, vol. 6, no. 9, pp. 7887–7900, May 2023. Available: https://doi.org/10.1021/ACSANM.3C01040

[41] Q. He, Y. Xu, and X. Yang, "Facile synthesis of aromatic porous organic polymer for highly selective capture of CO_2 via enhanced local dipole-π and dipole-quadrupole interactions by adjacent benzene," *Polym. Sci. - Ser. B*, vol. 61, no. 5, pp. 629–636, Sep. 2019. Available: https://doi.org/10.1134/S1560090419050063

[42] J. Liu *et al.*, "High-density and super ultra-microporous-activated carbon macrospheres with high volumetric capacity for CO_2 capture," *Adv. Sustain. Syst.*, vol. 2, no. 2, Feb. 2018. Available: https://doi.org/10.1002/adsu.201700115

[43] D. H. Jeon, S. T. Bae, and S. J. Park, "Preparation and characterization of chemically activated carbon materials for CO_2 capture," *Carbon Lett.*, vol. 17, no. 1, pp. 85–89, Jan. 2016. Available: https://doi.org/10.5714/CL.2016.17.1.085

[44] J. F. Vivo-Vilches *et al.*, "Resorcinol–formaldehyde carbon xerogel as selective adsorbent of carbon dioxide present on biogas," *Adsorption*, vol. 24, no. 2, pp. 169–177, Feb. 2018. Available: https://doi.org/10.1007/S10450-018-9933-6

https://doi.org/10.24191/esteem.v21iMarch.4713.g3055